Exploring impedance spectroscopy as a mean of malaria diagnostic

Simão Nunes Paula

Under supervision of Raul Carneiro Martins and Doutora Maria de Fátima Carvalho Nogueira

IST, Lisbon, Portugal

November 2014

Abstract

Malaria is an infectious disease caused by the parasites from the *Plasmodium* spp. genus and presents problems associated with its treatment and diagnosis. In the present work, it is analyzed the hemozoin crystal's characteristics (morphology, size and electric properties) obtained from different processes – natural source (*P. falciparum* strains 3D7 and Dd2) and synthetic sources and explored the possible use in malaria treatment. Furthermore, impedance spectroscopy (IS) was tested as a possible malaria diagnosis technique.

Hemozoin crystals, from natural and synthetic sources, were analyzed using different techniques, such as electronic microscopy (SEM and TEM) and impedance spectroscopy. The analysis of impedance measurements in healthy and infected red blood cells (RBCs) by *P. falciparum* Dd2 and 3D7 strains were made containing different developmental stages (ring, trophozoite, schizont).

Even though the characteristics between synthetic and natural crystals are different, one of the protocols for synthetic hemozoin produced crystals with properties closer to the natural hemozoin. The impedance measurements made in infected –RBCs with different *P. falciparum* stages were indeed different from the impedance measurements in uninfected-RBCs and demonstrated that it is possible to distinguish infected from uninfected blood samples.

These results support the idea that it is possible to approach both crystals formation processes thus simultaneously contributing to the production of antimalarial drugs able to diminish the parasite resistance. We also demonstrate that it is possible to use impedance measurements directly on blood to distinguish non-infected blood from malaria-infected blood which can be used for future development of a label-free diagnostic test.

Keywords: hemozoin characterization, malaria diagnostic, *Plasmodium falciparum,* scanning electron microscopy (SEM), transmission electron microscopy (TEM), impedance spectroscopy (IS)

1. Introduction

Malaria infection is caused by the protozoan parasites of the genus *Plasmodium* spp. and can be identified by 5 species, *Plasmodium falciparum*, *Plasmodium vivax*, *Plasmodium ovale*, *Plasmodium malariae* and *Plasmodium knowlesi*. *Plasmodium falciparum* is transmitted by mosquito *Anopheles gambiae* and it is responsible for the most severe infections, triggering several cases of human mortality [1-3]. *Plasmodium's* life cycle is constituted by two phases, the sexual reproduction cycle phase (occurs on the vector mosquito), and the pre-erythrocytic and intraerythrocytic phases (occur on the human host) [4]. In intraerythrocytic phase, malaria parasite digests large

quantities of host hemoglobin as a major source of amino acids. The degradation process triggers the release of a substance toxic to the parasite, heme (ferriprotoporphyrin IX) [5, 6]. The released heme suffers oxidation in order to produce hematin (aqua / hydroxyferriprotoporphyrin IX), which is then transformed into a crystalline substance, called malaria pigment or hemozoin. This transformation is given the name of biocrystallization, a detoxification process of parasite [7-11]. About 95% of the hematin used in this process is converted to hemozoin [12], which is not toxic for the parasite [6].

Fitch and Kanjananggulpan have suggested that hemozoin is composed by iron (III) protoporphyrin IX (Fe III) PPIX, which has a similar structure to an insoluble precipitate Fe (III) PPIX, synthetic β-hematin [13]. In 1991, through techniques like X-ray diffraction, infrared spectroscopy, and solubilization studies, it was proved that β-hematin was identical to hemozoin [14]. Later in 1997 was applied the technique synchrotron radiation X-ray powder diffraction and proved which hemozoin had an identical diffraction pattern of β-hematin [6, 15]. In 2005 was applied a technique of synchrotron radiation X-ray powder diffraction to analyze crystals formed by *Schistosoma Mansoni* and *Rhodnius Prolixus*, subsequently proving that the structures obtained by Rietveld Refinement and their own were a match. These structures were then compared to the structures of β-hematin. The result of this study was the achievement of very similar values, thus confirming that β-hematin and the natural crystals shared the same unit cell and structure [16, 17].

Native and synthetic (β-hematin) hemozoin can also be characterized by their physical properties [16]. The scanning and transmission electron microscopy have demonstrated that the crystal has well-defined faces [18] with 0.2-1.6 μm in size [6, 19]. Hemozoin is also birefringent, which is the capacity to depolarize light, thus allowing its detection by dark-field and polarization microscopy [20]. Determining the external macroscopic morphology of the crystal (crystal habit) is important for the molecular understanding of the mechanism of hemozoin formation[19, 21]. The study and identification of the factors involved in the inhibition of the detoxification process of the parasite will be important for the clinical assays of new drugs. The optimization of the factors will allow for an environment greater efficiency during the assays, and possibly the development of antimalarials less prone to resistance by the parasite [8, 22-24]

Malaria diagnosis involves identifying malaria parasites (parasitemia) or antigens/products in patient blood. Several factors can influence the identification and interpretation of malaria parasitemia in a diagnostic test (different stages of erythrocytic schizogony, the endemicity of different species, the interrelation between levels of transmission, population movement, parasitemia, immunity, drug resistance, persisting viable or non-viable parasitemia, sequestration of the parasites in the deeper tissues, and the use of chemoprophylaxis) [25]. The search for new diagnostic techniques which can reduce the interpretation error and that can identify the disease efficiently is of the utmost importance [25]. One of the biggest reasons for the need of innovation in testing equipment and diagnosis is the detection of severe malaria caused by the parasite *P. falciparum*, particularly cerebral malaria [26]. The infected red blood cells by *P. falciparum* have the ability of connecting themselves with the vascular endothelium through a process called cythoadherence. As a consequence sequestration phase of red blood cells (RBCs) occurs containing mature forms, early trophozoite stage (Fig. 1.1 B) to schizont stage (Fig. 1.1 C) of the parasite in organs (heart, lung, brain, liver, kidney, subcutaneous tissues and placenta). The

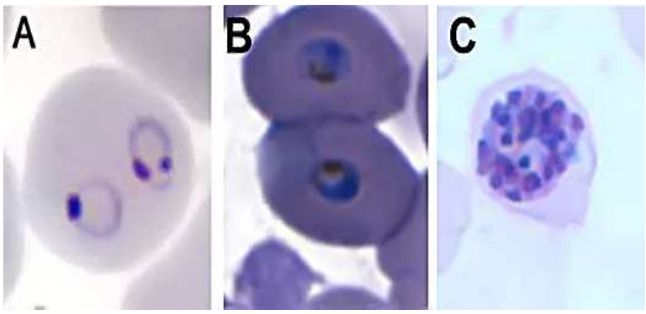

Figure 1.1 – Stages of malaria parasite on thin blood smear. This thin film Giemsa-stained micrographs reveals ring-stage (A) trophozoite-stage (B) and schizont-stage (C) of *Plasmodium falciparum* [27]

Plasmodium falciparum-infected RBCs with mature forms are no longer detectable in peripheral blood smears, complicating the diagnosis. Only infected red blood cells at the ring stage (Fig. 1.1 A) will circulate on the peripheral blood and might be detected [3, 28-30].

In this study crystals of β-hematin (synthetic hemozoin) and native hemozoin were produced and analyzed for direct comparison between their microstructural features and passive electrical properties, with the purpose of finding their role and importance in inhibition of the detoxification process of the parasite through of antimalarial drugs. Moreover, it was explored the possibility of an innovative method for malaria diagnosis through application of impedance spectroscopy (IS). This analytical technique can characterize the electrical properties of biological materials [31], like *Plasmodium falciparum*-infected red blood cells (*Pf*-RBCs) and uninfected red blood cells (uRBCs). The electrical properties analyzed may be able to distinguish blood infected as well as not infected by malaria, and maybe apply this technique as RDT (Rapid Diagnostic Test).

2. Materials and Methods

2.1. Production of synthetic hemozoin (β-Hematin)

2.1.1. Protocol 1

Prepared using a modified protocol of Slater *et al.* as follows [32]. After prepared 4.5 ml of hemin solution, was transferred 1 ml of solution to each four different tubes properly marked. The hemozoin polymerizations were initiated by addition to each tube of 350 µl of glacial acetic acid (Sigma) and by heating at 80ºC overnight (approximately 12 hours) in heating block. The following day, tubes with pellet, synthetic hemozoin (sHz), were washed four times in ultra-pure water (Milli-Q) centrifuged at 3300 xg for 15 min. and washed again two times for 3 hours in sodium bicarbonate solution with pH 9.1 and centrifuged at 3300 xg for 15 min. Finally tubes with pellet were washed four additional times in ultrapure water (Milli-Q) centrifuged at 3300 xg for 15min., resuspended in 1 ml of PBS solution. The heme-equivalent of crystals has been determined from interpolation using standard hemin solution absorbances determined with a TRIAD Series LT Multimode Detector (Dynex Tecnologies), using a calibration curve. Synthetic hemozoin was stored at 4ºC.

2.1.2. Protocol 2

After preparing 5 ml of hemin solution, 1 ml of solution was transferred to each five different tubes properly marked. The hemozoin polymerizations were initiated by addition to each tube of 150 µl of ultrapure water and 150 µl of glacial acetic acid (Sigma) and incubation at 37º C overnight (approximately 24 hours). The following day, tubes with pellet, synthetic hemozoin (sHz), were centrifuged at 3300 xg for 15 min. and the supernatant discarded. Afterwards, the pellet was resuspended in 1 ml of DMSO (Sigma) and centrifuged at 3300 xg for 15 min. The previous process was repeated five and six times until supernatant becomes translucent. Finally, pellet was washed two times in ultrapure water (Milli-Q) by centrifuging at 3300 xg for 15 min and resuspended in 1 ml of PBS solution. The heme-equivalent of crystals has been determined from interpolation using standard hemin solution absorbances determined with a TRIAD Series LT Multimode Detector (Dynex Tecnologies), using a calibration curve. Synthetic hemozoin was stored at 4ºC.

2.2. Production of native hemozoin

2.2.1. Preparation of non-parasitized red blood cells

From healthy human donors was harvested 10 to 20 ml of venous blood (plus EDTA) - free of any kind of medication. Each sample is divided in 5 ml aliquots and centrifuged at 950 xg for 5 minutes in order to remove the leukocytes blood fraction. In order to wash the erythrocytes, the 10 ml of incomplete RPMI medium (without AlbuMaxII) were added to each sample followed by mixing through inversion. The mixture was centrifuged at 950 xg for 5 min. The supernatant was removed and this washing step was repeated two to three times.

To the final erythrocytes pellet was added 10 ml of (completed) RPMI medium. The erythrocytes cell suspension (50%) was preserved at 4°C during, a maximum, of 15 days.

2.2.2. In vitro culture of Plasmodium falciparum

In vitro culture growing of *P. falciparum* clones, was performed according to Trager & Jensen (1976) [33], Thaithong *et al.,* (1994) [34] and Cranmer *et al.,* (1997) [35] with some modifications. In order to grow this type of *Plasmodium*, erythrocytes were maintained in RPMI culture medium at 37°C with a 5% of CO_2. The hematocrit was considered to be 5%. The parasite development was assessed through the observation of blood smears stained with 20% Giemsa (Merck) using an optical microscope. When parasitemia reached 5 to 8% of infected erythrocytes, new dilutions and new cultures were made.

2.2.3. Extraction of native hemozoin from parasite cultures

P. falciparum (strain 3D7 and Dd2) hemozoin (or native hemozoin, nHz) was extracted of frozen culture with high parasitemia of trophozoites and schizonts. First, frozen cultures were washed one time in ultra-pure water (Milli-Q) centrifuged at 1900 xg for 10 min. and the supernatant aspirated. The pellet obtained was added to 10 ml of saponin solution (Sigma) and incubated at 37ºC until lysis was complete. After centrifuging at 1900 xg for 10min., the pellet was washed four times in ultra pure water centrifuged at 6600 xg for 5min., sonicated in 2% SDS (≈ 2min), washed four times with 2% SDS by centrifuged at 6600 xg for 5 min and then incubated overnight at 37ºC with solution A. After being washed two times with 2% SDS and undergoing centrifugation (6600 xg for 5min), the pellet was incubated in 6 M urea solution at room temp in an agitator for 6 hours and then washed two times with 2% SDS and two times with ultrapure water (Milli-Q) centrifuged at 6600 xg for 5min. Purified nHz was resuspended in 500 µl of ultrapure water. The heme-equivalents were determined by interpolation of standard hemin solution absorbances (read in TRIAD Series LT Multimode Detector (Dynex Tecnologies), using a calibration curve. Purified nHz was stored at 4ºC.

2.3. Scanning Electron Microscopy (SEM)

SEM was used to observe of the morphology of sHz and nHz crystals in order to characterize their shape, size and structure. On top of metallic sample holder were placed 10 µl of nHz and sHz resuspended in ultrapure water (Milli-Q) and allowed to dry 3 to 4 hours in room temp, using artificial light for acceleration of the drying process. Then, the specimens were coated two times with a carbon layer in a Q150R Rotary-Pumped Sputter Coater/Carbon Coater and they were examined in a JEOL 7001F field emission scanning electron microscope, at *Instituto Superior Técnico*, using an accelerating voltage of 15.0 kV. Secondary electron images were acquired while operating the microscope in a low vacuum mode by digital photo documentation system.

2.4. Transmission Electron Microscopy (TEM)

TEM was used for the analysis of the microstructure of the sHz and nHz crystals in order to characterize their shape, size and structure. On top of mounting grid with absorbent paper underneath were dropped 10 µl of nHz and sHz resuspended in ultrapure water (Milli-Q) dispersing the crystals of hemozoin. The hemozoin was allowed to dry at room temperature. Since the solvent does not react with the sample material only the hemozoin crystals were left in the grid. Then, the grid was inserted in Gatan TEM sample holders and examined in Hitachi H8100 transmission electron microscope, at Instituto Superior Técnico, using an accelerating voltage of 200 kV. Bright-field images were acquired by digital photo documentation system.

2.5. Impedance Spectroscopy (IS)

2.5.1. Measurement Principle

In this present work, two different impedance spectroscopy devices were used. The first one has the ability of reading low frequencies, Ifreq ∈ [10 kHz – 82.5 kHz], and the second one was the ability of reading high frequencies such as [freq ∈ [250 kHz – 5 MHz]. The principle underlying the operation of both devices is the same being the read frequencies the only distinction. Its operation is presented in Fig. 2.1.

The input signal of the circuit (Fig. 2.1) is a voltage (Vi) (1) which is converted to an output current (Io) (2) due to the transcondutance amplifier. With the increasing of the signal's frequency, the current (Io) is applied to the sample being analyzed (5) by two electrodes (3). At the same time, a voltage (V) is measured in the same sample (4). The resulting impedance is measure by a potential difference and will correspond to the electrical resistance (R), according to Ohm's Law

(equation 1). Since the signal obtained has low amplitude, its value (real data) is amplified using an instrumentation amplifier (6) and then is quantized into binary data, Vimpedance (7).

With the high frequencies circuit a Crest Factor of 1.405 for excitation signal was used in order to normalize the amplitude of the signal to the peak-to-peak values of the sine wave, thus allowing for a better discretization of the signal.

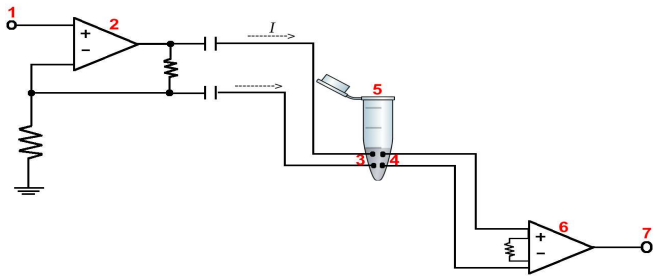

Figure 2.1 – Measurement principle of impedance spectroscopy for low and high frequencies devices.

2.5.2. Synchronization of in vitro cultures of Plasmodium falciparum

Since all *P. falciparum* development stages (rings, trophozoites, schizonts and occasionally gametocytes) were observed during in vitro culture of erythrocytes it is important to achieve synchronization of the cultures before the execution of impedance spectroscopy assays.

The osmotic fragility of malaria-infected erythrocytes is known to increase during the development of the parasite [36, 37]. Based in this observation, synchronization was achieved by applying an osmotic shock to erythrocytes using sorbitol (5%) for that purpose [38]. Cultures presenting a 10% level of parasitemia, with predominance of young parasites, were centrifuged (676 xg during 5 minutes). The supernatant was discard and to the pellet were added 10 volumes of 5% D-Sorbitol (Merck) previously sterilized by filtration (0.2 µm filters, Millipore). After 10 minutes of incubation at 37°C, the mixture was centrifuged and washed twice with RPMI (without plasma). The erythrocytes pellet, recovered after the last centrifugation, was resuspended in the already stated culture conditions. If required, this protocol can be repeated 6 to 8 hours later.

2.5.3. Non-parasitized and parasitized red blood cells assays

Having in mind the culture parasitemia calculated can proceed to the non-parasitized and parasitized red blood cells assays. For that purpose, two different tubes were prepared: A – RBCs parasitized with *P. falciparum* (strain 3D7 or Dd2) and B – healthy RBCs thus being non-parasitized (control).

Each tube with RBCs parasitized was submitted to four different conditions: the first one was an assay in culture medium (RPMI) with all parasite stages present (1A); the second one was an assay performed in culture medium (RPMI) but just with ring stage (2A); the third one was an assay performed in Whole Blood (WB) from the donor in which were present all parasite stages (3A); a four assay performed in Whole Blood (WB) from the donor synchronized for the ring stage (4A); the last assay was performed again in WB but this time it was synchronized for the schizont stage (5A).

Each mixture was then consecutively diluted (1:2) six to eight times with RPMI + uninfected RBCs (1A and 2A) or WB (3A, 4A and 5A). Finally, using the previously built impedance spectroscopy devices (Fig. 2.1), the non-parasitized and parasitized red blood cells assays were analyzed in two different electrodes configuration (parallel and cross) by reading their phase (θ) and amplitude (Ohm). Through the data obtained we proceeded to the construction of Nyquist plots.

2.5.4. Hemozoin crystals assays

In order to analyze both samples, two distinct tubes were prepared, in PBS buffer, containing sHz (protocol 1 and protocol 2) with an equal concentration, in terms of heme equivalents, as the nHz. Successive dilutions (1:4) were made from each tube using PBS buffer as solvent. Finally, using the previously built impedance spectroscopy devices, the nHz and sHz assays were analyzed in two different electrodes configuration (parallel and cross) by reading their phase (θ) and amplitude (Ohm). Through the data obtained we proceeded to the construction of Nyquist plots.

3. Results

3.1. SEM analysis (hemozoin crystals)

In Figure 3.1 it is possible to observe images obtained through SEM with different magnifications, where A (1, 2 and 3) corresponds to micrographs of the nHz from *P. falciparum* strain 3D7's; B (1, 2 and 3) corresponds to micrographs of the nHz from *P. falciparum* strain Dd2's; C (1, 2 and 3) corresponds to micrographs of β-hematin chemically synthesized (sHz) using protocol 1; D (1, 2 and 3) corresponds to micrographs of β-hematin chemically synthesized (sHz) using protocol 2.

On micrographs A1, A2 and B2 it can be observed the heterogeneity of the crystals size, showing a very regular form. Its morphology exhibits very well defined faces, with flat and smooth shapes. Moreover, some crystals present large shapes and some small ones as well, with lengths ranging from 0.2 µm to 1.4 µm, and width ranging from 100nm to 500 nm. During the observation of these crystals on SEM it was possible to verify that they easily aggregate to each other, as it can be seen in micrographs A1, A2 and B2. In the right side of micrograph B2 it can be found a structure of crystals with brick-like shapes. Notably, in micrograph A3 and B3 it can be observed two crystals with a uniform shape on its sides, similar to parallelepiped, with length 1.6 µm and width 300 nm (A3), and length 1.4 µm and width 200 nm (B3). Some crystals contain membranes and proteins aggregated which weren't completely removed during the process of extraction and purification to the nHz (A1 and B2).On the micrographs of protocols 1 and 2 it can be observed the heterogeneity of the different sizes of the crystals. Micrographs D corresponding to protocol 2 show less heterogeneity in crystals. The micrographs C show the presence of some thinner crystals and micrographs D show larger crystals. All micrographs crystals show lengths ranging from 0.2 µm to 1.5 µm, and width ranging from 80 nm to 250 nm. Notably, the shape of some crystals is more extended in different directions, like a needle, as it can be observed in micrographs C and D. Moreover, these crystals showed similarities with parallelepiped but with some irregularities in its shape.

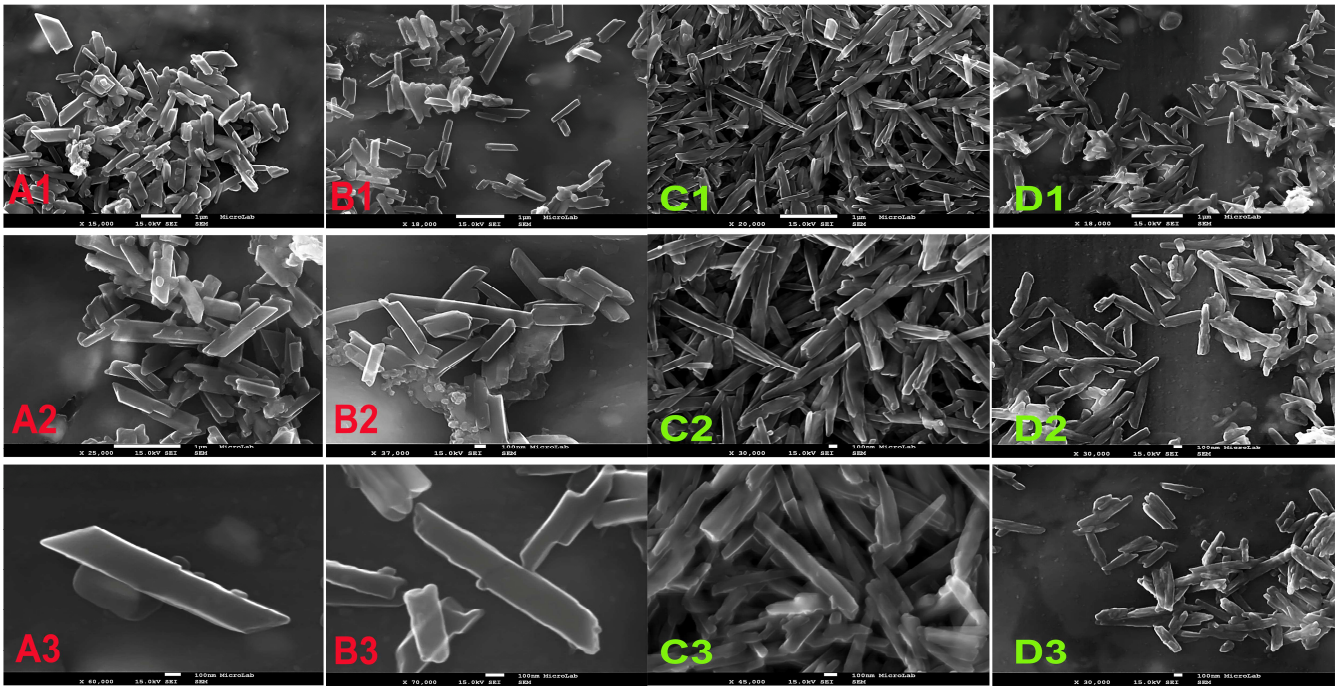

Figure 3.1 - Electron micrographs showing heterogeneity of shape and size for crystals of native and synthetic hemozoin. FEG-SEM images (SEs) of hemozoin from *P. falciparum* strain 3D7 (A1, A2 and A3) and Dd2 (B1, B2 and B3), and of synthetic hemozoin produced from Protocol 1 (C1, C2 and C3) and Protocol 2 (D1, D2 and D3) for different magnifications.

3.2. TEM analysis (hemozoin crystals)

In Figure 3.2 it is possible to observe images obtain through TEM with different magnifications, where E (1, 2, 3 and 4) corresponds to micrographs of the nHz from *P. falciparum* strain 3D7's; F (1, 2, 3 and 4) corresponds to micrographs of the nHz from *P. falciparum* strain Dd2's; G (1, 2 and 3) corresponds to micrographs of β-hematin chemically synthesized (sHz) using protocol 1; H (1, 2 and 3) corresponds to micrographs of β-hematin chemically synthesized (sHz) using protocol 2.

On micrographs E1 and F1 a great heterogeneity of crystals' size can be observed, with length ranging from 0.3 μm to 1.4 μm, and width ranging from 100 nm to 400 nm. Like in SEM, in every micrograph the crystals present a well-defined morphology with regular plane faces similar to those of a parallelepiped. In micrograph F1 it can be observed that the crystals´ microstructure shows up worn at the edges of its faces thus originating shapes more rectangular than parallelepiped, as well as crystals with brick-like shapes with different dimensions and located on the right side of the micrograph. In micrographs E2 and F2 the increased magnification allowed for a better observation of the microstructures, taking the morphology of a parallelepiped. Adopting this morphology, the dimensions for crystals in E2 are 900 nm x 200 nm x 100 nm, and for the ones in F2 the dimensions are 700 nm x140 nm x 50 nm (1) and 790 nm x 150 nm x 50 nm (2). The two micrographs, E4 and F4, correspond to the magnification of the faces' edges of the crystals shown in micrographs E2, E3 and F3, which allow for their microstructure to be observed in great detail. In this area it is possible to see that the crystal is organized in several layers (indicated by the yellow arrow) evenly distributed along a diagonal line.

For the different synthetic hemozoin crystals shown in micrographs G1 and H1, it can be observed the heterogeneity in their shape and size, this being greater for G1. Long and thin shapes, similar to a blade or a needle, are observed on the crystals in micrographs G, with length ranging from 0.14 μm to 1.8 μm, and width ranging from 40 nm to 150 nm. On the same micrographs there are some crystals that show plane faces and with more uniform surfaces on the sides. In micrographs H frequently observed crystals with more regular shapes and plane faces, similar to a parallelepiped or a rectangle. There are also in these micrographs crystals shaped like needles, although they are less frequent. The crystals in micrographs H have lengths ranging from 0.18 μm to 1.25 μm, and width ranging from 50 nm to 150 nm. By observing the microstructure of the crystals at higher resolutions, like in micrographs G2, G3, H2 and H3, it is verified that their organization has no layers and that there is some irregularities in their shaping.

3.3. IS analysis

The samples of hemozoin and uRBCs and *Pf*-iRBCs were analyzed using two identical devices but with different

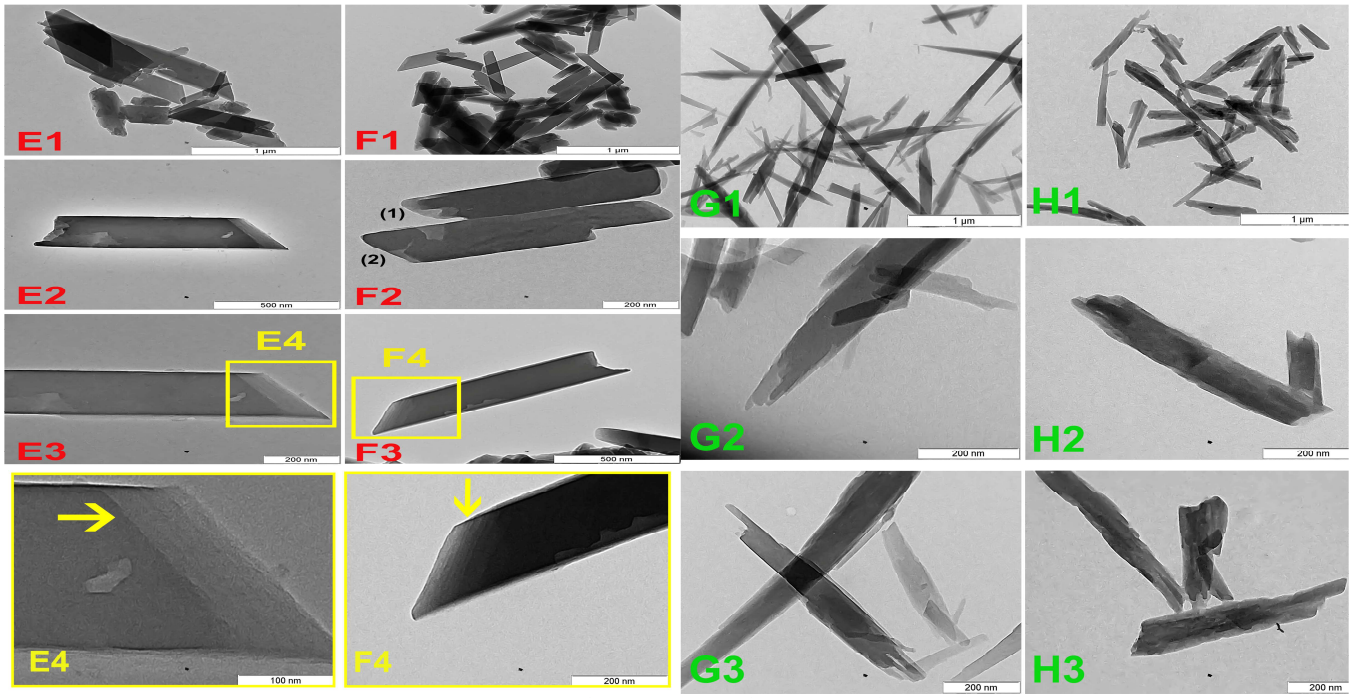

Figure 3.2 - Electron micrographs showing heterogeneity of shape and size for crystals of native and synthetic hemozoin. TEM bright-field images of hemozoin from *P. falciparum* strain 3D7 (E1, E2, E3 and E4) and Dd2 (F1, F2, F3 and F4), and of synthetic hemozoin produced from Protocol 1 (G1, G2 and G3) and Protocol 2 (H1, H2 and H3).

ranges for the frequency of the excitation signal - one with a high frequency range, the other with a low frequency range - and likely to operate in the traditional tetrapolar configuration for impedance measurement with variable arrangement of electrodes, crossed and parallel.

3.3.1. *Hemozoin Crystals*

The following are overlapped Nyquist graphs are ordered from 1 (highest concentration) to 5 (lowest concentration), in order to analyze the evolution of the impedance with the decreasing of the concentration of the native and synthetic crystals in a PBS environment, and at the same time compare and characterize the passive electric properties of the different hemozoin crystals.

The qualitative analysis of the Nyquist graphs for low frequencies in a crossed configuration shows that the evolution of the impedance curves exhibits a large discrepancy in electrical resistance and reactance with the decreasing concentration, without any coherence. In the parallel configuration the evolution of the impedance curves of the crystals remained unchanged with decreasing concentration (results not shown). The qualitative analysis of the Nyquist graphs for high frequencies, Ifreq ∈ [250 kHz – 5 MHz], shows that the evolution of the impedance curves exhibits a greater coherence. For the crossed configuration (Fig. 3.3 A), nHz and sHz P2 show impedance curves in which the electrical resistance and reactance decrease with the decreasing concentrations over the graphs (1 to 5). However, sHz P1 impedance curves show that there is an increase (5) in electrical resistance while at the same time a decrease in reactance with the decreasing concentrations over the graphs (1 to 5). With the evolution of the graphs (1 to 5) is it possible to observe the approach of the impedance curves of nHz, and sHz P1 and P2, to the impedance curve of the PBS (white) (5). The impedance curves of nHz and sHz P2 almost overlap and they also present an identical evolution in terms of reactance and electrical resistance (1 to 5), which makes this the most noticeable result on the graph showing a concentration of 0.337 mM (2). Although some impedance curves of sHz P1 also overlapping the curves of nHz and sHz P2 (1 to 5), these however show some inequality in its evolution.

In the parallel configuration of the electrodes (Fig. 3.3 B), it can be verified that the evolution of the graphs of nHz and sHz P1 and P2 are similar to those of the crossed configuration, but with impedance curves that exhibit higher reactance and electrical resistance, that are very slowly approaching the impedance curve of the PBS (white) (1 to 5). In the impedance curves nHz and sHz P2 reactance does not vary much, however the electrical resistance shows a slight decrease with the decreasing concentration over the graphs (1 to 5). Again, it is possible to observe strong similarities and greater overlapping in the impedance curves of nHz and sHz P2 (1 and 2) than what is observed in the crossed configuration curves. As in the crossed configuration, impedance curves of sHz P1 show decreasing reactance (1 to 5) and an increase in electrical resistance (1 and 5) as the concentration decreases over the various graphs (1 to

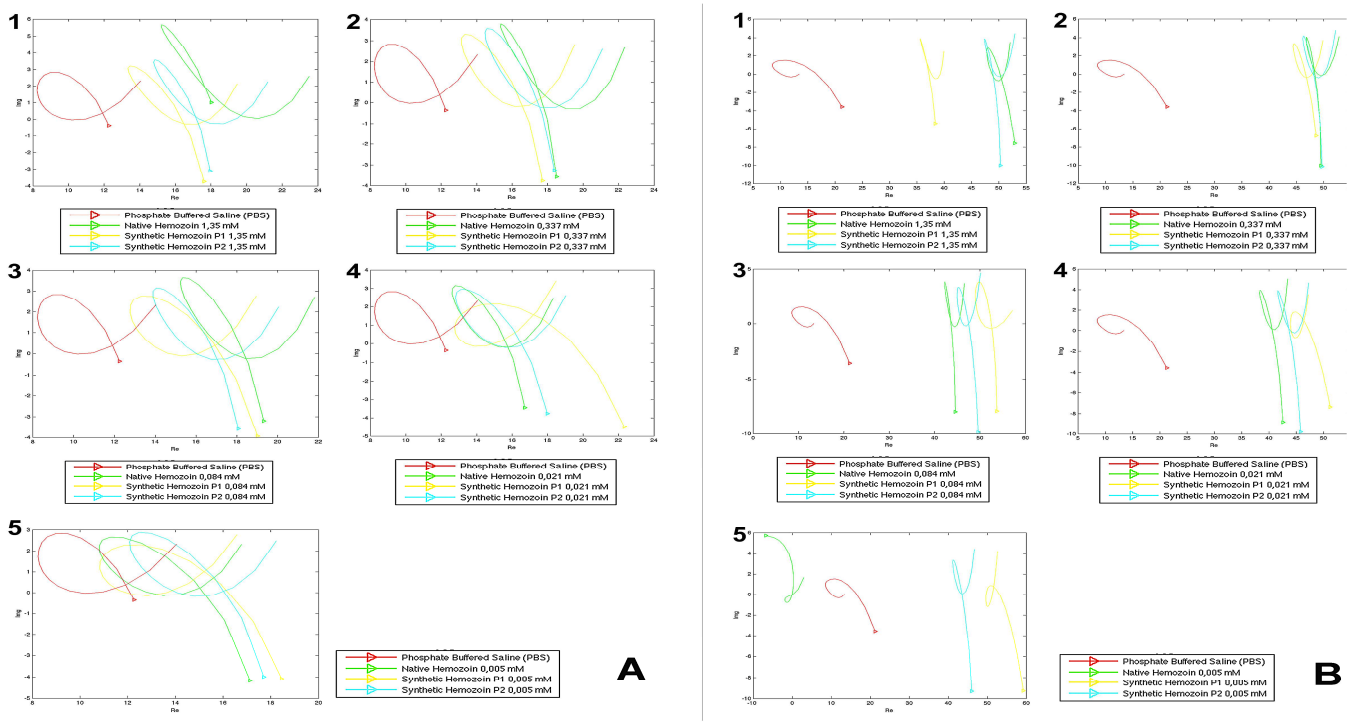

Figure 3.3 - Nyquist plots of impedance spectroscopy for native (*P. falciparum* strain Dd2) and synthetic (Protocol 1 and 2) hemozoin crystals assays with high frequencies device, $I_{freq} \in$ [250 kHz – 5 MHz], using electrodes in cross (A) and parallel (B) configuration. The nyquist plots overlaid on the image shows the variation of impedance in function of a frequency response for hemozoin (nHz and sHz) suspensions concentrations in PBS (white). Concentrations 0.337 mM (2), 0.084 mM (3), 0.021 mM (4) and 0.005 mM (5) were obtained from successive dilutions 1:4 an initial concentration of 1.35 mM (1). The initial value of the impedance and of the lower frequency (250 kHz) is represented by the symbol **Δ** in each plot**.** The Nyquist plot has a Real part (x axis), equivalent to electrical resistance in Ohms, and an Imaginary part (y axis), given by reactance in Ohms, which together constitute the impedance.

5), presenting a great inequality and without much overlap in relation to the impedance curves of nHz and sHz P2.

3.3.2 Non-parasitized and parasitized red blood cells assays)

On the first assay of the impedance obtained from testing mixtures of uRBCs and *Pf*-iRBCs with all stages of the parasite and only with a unique stage (ring or schizont) of the parasite by *P. falciparum* 3D7 strain in RPMI and in WB, it is possible to verify that in the low frequency range, $I_{freq} \in$ [10 kHz – 82.5 kHz], for a crossed configuration the impedance curve present very incoherent evolution paths. On the contrary, for the parallel configuration, the impedance curves exhibit more coherence and a more logical path of evolution, without presenting a good distinction between them. According to the values of impedance obtained in the high frequency range, Ifreq ∈ [250 kHz – 5 MHz], for the different mixtures, it is possible to verify that in both configurations there is some coherence and an increase in the discrimination between the impedance of the curves (results not shown).

After observation of the results obtained in the first assay of impedance spectroscopy, was performed one second assay in mixtures of *Pf*-iRBCs (strain Dd2) and uRBCs in RPMI and WB. For the new assay, it was decided to use only the device capable of measuring the high frequency range of the excitation signal.

In a general and qualitative analysis of the results obtained for the impedance of the mixtures containing all stages (Fig. 3.4 A and Fig 3.5 A) and the ring stage (Fig. 3.4 C and Fig. 3.5 C), both in a RPMI medium using crossed and parallel configuration, it is possible to observe that the impedance of the *Pf*-iRBC's curves increases with the increasing percentage of parasitemia and in relation to the impedance of the control curve. The discrimination between the values of impedance of the control curve and *Pf*-iRBC's curve is greater for parasitemia over 0.5%. Comparing the results obtained for both configurations, it is observable an increase in discrimination and stability as well when a parallel configuration is applied (Fig 3.5 A and C). However, the assay with a mixture containing the stage ring done in a crossed configuration (Fig. 3.4 C), show that the impedance of the *Pf*-iRBC's curve doesn't increase with the increasing parasitemia, which is contrary to what was expected. The results obtained in a WB medium shows that the impedance of the *Pf*-iRBC's curves increases with the increasing percentage of parasitemia and in relation to the impedance of the control curve (Fig 3.4 B and D, and Fig. 3.5 B and D). In addition, the impedance of the *Pf*-iRBC's curves present a good discrimination from the lowest percentage of parasitemia, 0.031%. In all assays, both the crossed and parallel configurations allowed for

stable results; however the crossed configuration showed a better discrimination of the impedance values between the *Pf*-iRBC's curves and the control curve (Fig 3.4 B and D).

4. Discussion

4.1. Hemozoin Crystals

Hemozoin remains a good source for continuous search for new anti-malarial drugs (in vitro assays), which inhibit the formation process of crystals via synthetic route [5, 20, 22, 39, 40]. However, the experimental conditions of the synthetic crystals production are difficult to control, which causes differences between the formation process of synthetic and natural crystals. It is not yet proven that hemozoin crystals synthetically obtained are really equal to the naturally obtained ones.

In the results obtained for different micrographs in SEM and TEM, it is possible to verify that crystals showed habits in their shape (Fig. 3.1 to 3.2), as already reported in previous studies [16, 41].

Correlating the results of micrographs for crystals nHz of strain 3D7 and Dd2 (Fig. 3.1 A and B, Fig. 3.2 E and F), it is observed that these show shapes with the same habits, mostly parallelepiped, with well-defined faces and with similar size with nm and µm dimensions, which indicates that regardless of the strain, the biocrystallization process of the heme in hemozoin by the parasite *P. falciparum* is identical. However, for the resistant strain Dd2 there are some crystals with brick-like shapes aggregated to each other in an organized fashion. This result is in agreement with results from previous studies on the characterization of nHz obtained from *P. falciparum* [19, 42]. Taking into consideration the result of micrographs of hemozoin crystals synthetically obtained by protocol 2 (Fig. 3.1 D have two types of forms. The first one is a needle-like shape, with long length and thin width; the second is a parallelepiped shape, with smaller length but with width similar to the needle-like shape. Nevertheless the needle-like shape is more visible in the crystals obtained with protocol 1 (Fig. 3.1 C and Fig. 3.2 G) than with protocol 2. Noticeably, the crystals obtained with protocol 2 appear to be more evenly spread than the ones obtained with protocol 1, which shows a greater heterogeneity. These results indicate that the experimental process for production of sHz for protocol 2 leads to crystals with a more controlled and homogeneous morphology and size.

By comparing micrographs of nHz 3D7 and Dd2 strains (Fig. 3.1 A and B, Fig. 3.2 E and F), with the micrographs of crystals of sHz obtained with protocols 1 and 2 (Fig. 3.1 C and D, Fig. 3.2 G and H), it is verifiable that the shapes and sizes of the crystals produced with protocol 2 shows similarities with the nHz crystals

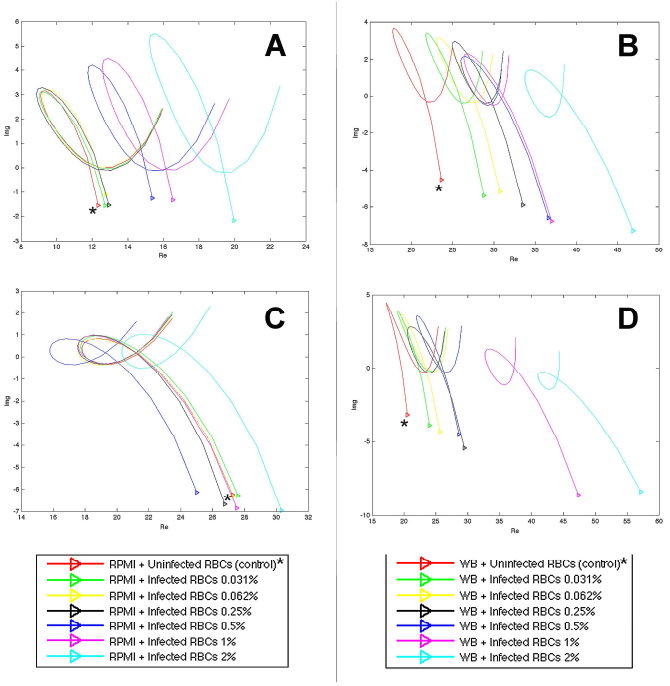

Fig. 3.4 - Nyquist plots of impedance spectroscopy for non-parasitized and parasitized (by *P. falciparum* strain Dd2) RBC´s assays generated with high frequencies device, $I_{freq} \in$ [250 kHz – 5 MHz], and electrodes in cross configuration for : A) unsynchronized culture**, B)** unsynchronized infected whole blood**, C)** ring-synchronized culture and **D)** ring-synchronized infected whole blood.

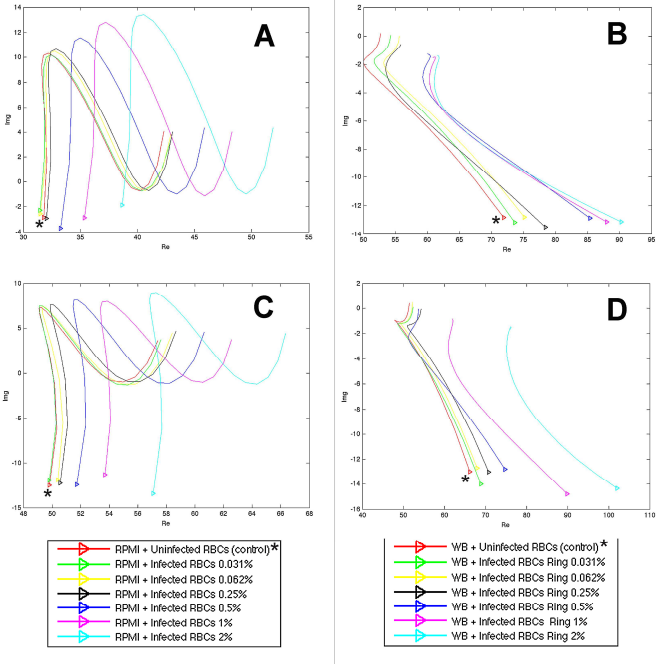

Fig. 3.5 - Nyquist plots of impedance spectroscopy for non-parasitized and parasitized (by *P. falciparum* strain Dd2) RBC´s assays generated with high frequencies device, $I_{freq} \in$ [250 kHz – 5 MHz], and electrodes in cross configuration for : A) unsynchronized culture**, B)** unsynchronized infected whole blood**, C)** ring-synchronized culture and **D)** ring-synchronized infected whole blood.

The Nyquist plots overlaid on the images (**Fig 3.4 and 3.5**) show the variation of impedance as function of the frequency response for different percentages of infected RBCs and for uninfected RBCs. The prepared mixtures of infected and uninfected RBCs have a hematocrit ≈ 45% in WB and ≈ 5% in RPMI. In the figure, an asterisk (*) identifies the control curve, and the symbol **Δ** represents the initial value of the impedance and of the lower frequency (250 kHz) in each plot. The Nyquist plot has a Real part (x axis), equivalent to electrical resistance in Ohms, and an Imaginary part (y axis), given by reactance in Ohms, which together constitute the impedance.

produced by *P. falciparum*. Moreover, the shapes and sizes of the crystals obtained with protocol 1 show a greater distinction from the nHz crystals. This result proves once again that it is possible to control experimental conditions during the formation process of sHz (in vitro), in order to create synthetic crystals that share similar properties and characteristics with the nHz crystals.

In the TEM micrographs, obtained for higher resolutions, is verified that nHz crystals for both strains present layered structures on the faces of their tips, which show a uniform organization with parallelepiped shape (Fig. 3.2 E4 and F4). On the contrary, in protocol 1 most synthetic crystal have no layers in their tips and have the tendency to create a more tapered needle-like shape (Fig. 3.2 G). Notably, at higher resolutions, the crystals of protocol 2 demonstrate again parallelepiped shapes as in nHz crystals, although with some disruption in their structure and without any layers at the tips of the crystal's faces. These observations support the need to develop new protocols with controlled conditions which allow for the production of synthetic crystals with properties and characteristics similar to those of the native crystals.

According to the results obtained for the suspensions of nHz (strain Dd2) and sHz (Protocol 1 and Protocol 2), by impedance spectroscopy, for the low frequencies unit in crossed and parallel configuration cannot distinguish between the electrical properties of the crystals. The fact that the device measures in the low frequencies range, $I_{freq} \in$ [10 kHz – 82.5 kHz], can reduce the level of discrimination possible with the frequency response of the material analyzed, here the crystals. Moreover, in SEM micrographs (Fig. 3.1), some native and synthetic crystals have irregularities in their shape or aggregated materials in their structure (unpolymerized heme, membranes and proteins), and those factors might influence the actual measurements of the passive electrical properties of the crystals. The impedance results obtained using the high frequencies device, $I_{freq} \in$ [250 kHz – 5 MHz], for both configurations, suggest that the fact that the measures are taken in the high frequencies range cause an increase in the level of discrimination and thereby obtain a good frequency response of the crystals analyzed using impedance spectroscopy.

By analyzing the passive electrical properties as well as their evolution over the Nyquist graphs (Fig. 3.3), in ascending order (1, 2, 3, 4 and 5), it can be said that the nHz and sHz P2 crystals, for both configurations, show a greater reactance than in the case of sHz P1 crystals. This means that the material forming the nHz and sHz P2 crystals has a lower ability to disperse electric charge from the applied alternating current than the material of the sHz P1 crystals. However, for this evolution the sHz P1 crystals show greater resistive electrical properties, that is, the crystal structures have a higher charge transfer resistance with decreasing concentration in material resistivity, than for nHz and sHz P2 crystals. The fact that there are similarities in the passive electrical properties of nHz and sHz P2 crystals, for different electrode configurations, suggests that their formation processes are almost identical.

The challenge of applying this technique of impedance spectroscopy focuses on the differentiation of *Pf*-iRBCs with the ring stage from uRBCs [1, 43, 44]. However, IS technique can be an alternative to the PCR technique for the detection of submicroscopic infections, with the same efficacy but with an improvement regarding to the acquisition time of the results, thus functioning as a rapid diagnostic test (RDT) [45, 46]. According to the results of studies performed with the technique of impedance spectroscopy, the impedance of *Pf*-iRBCs increases with increasing parasitemia [43, 44].

In the results of first assay of the impedance obtained from testing mixtures of uRBcs and *Pf*-iRBCs with all the stages in RPMI and in WB, it is possible to verify that in the low frequency range, $I_{freq} \in$ [10 kHz – 82.5 kHz], it is difficult to distinguish the curve of uRBCs from the curve of *Pf*-iRBCs for both configurations. The inconsistencies as well as the low discrimination could be justified by the fact that the impedance measures are conducted at a low frequency range, which can lead to a bad signal response to the impedance of the cells. According to the values of impedance obtained in the high frequency range, $I_{freq} \in$ [250 kHz – 5 MHz], for the different mixtures, RPMI and WB, is noted that the discrimination is larger for the parallel configuration. From the results obtained for mixtures in WB, interestingly it is observed that for a crossed configuration present more coherent results. These results suggest that, in this case, the signal response of the cells' impedance is optimized for a crossed configuration when making measurements in the high frequency range, for a mixture in WB with various stages of the parasite.

The results of the impedance obtained from testing mixtures of uRBCs and *Pf*-iRBCs with the ring and the schizont stage in WB, in the low frequency range, for a crossed and parallel configuration the impedance of the curves obtained for the ring stage show many inconsistencies. As opposed to the impedance of the curves obtained for the schizont stage, which present coherence and distinction. The *Pf*-iRBCs with ring stage are non-mature cells of the malaria parasite and that still initially possess dielectric properties similar to those of the uRBC's membrane, such as capacitance. The membrane capacitance of the uRBCs shields the cell interior from the external electric field at low frequencies [43], which originates a non-existing or incoherent signal

response of the impedance of *Pf*-iRBCs with the ring stage. On the contrary, the *Pf*-iRBCs with schizont stage are mature cells resulting from the process of maturation of the malaria parasite, which causes striking structural and morphological changes in the *Pf*-iRBCs [26, 43, 44]. These changes lower the membrane's resistance and consequently the surrounding layer becomes less insulating [44]. The external electric field at low frequencies will be able to penetrate *Pf*-iRBCs with schizont stage thus originating a coherent response from its impedance. In the high frequency range, for the ring and schizont stage, it is demonstrate that for the two configurations in both stages there is consistency and an increase in the discrimination level between the impedance of the curves. At higher frequencies, owing to the short circuiting effect of membrane capacitance, the electric field penetrates to the cellular interior and reaches the parasite [43], thus optimizing the signal response of the impedance of *Pf*-iRBCs and uRBCs, obtaining at the same time better results.

Examining the results obtained from the second assay for impedance measurements obtained in the high frequency range, for all stages and ring stage of *Pf*-IRBCs strain Dd2 in RPMI and WB, it was observed an improvement in their stability and repeatability, indicated in figures 3.4 (A, B and D) and 3.5 (A, B, C and D). The stability and repeatability it is showed by the existence of a logical and coherent convergence of the impedance of the *Pf*-iRBC's curves towards the impedance of the uRBC's curve (control), with decreasing parasitemia. However, it is observed in figure 3.5 A, which represents the assay with the ring stage in the crossed configuration, an incoherent convergence of the impedance of the *Pf*-iRBC's curve towards the uRBC's curve, showing an incorrect variation on the value of the impedance with the increase of parasitemia. This result suggests that there are still errors associated with the experimental conditions or during the impedance measures. Furthermore, it indicates that the crossed configuration can contribute for measurement errors. Regarding the configurations for the different mediums, it is possible to observe that the parallel configuration allows for a better signal response of the impedance of cells in a RPMI medium (Fig. 3.5 A and C), thus obtaining an optimized discrimination between the impedance of the various curves. On the contrary, with the crossed configuration it is obtained a better response and discrimination in a WB medium (Fig. 3.4 B and D). Nevertheless, the results obtained show that both crossed and parallel configuration enables a distinction between the *Pf*-iRBC's curve (with all the stages or with just the ring stage) and the uRBC's curve. Another relevant factor, present in all the results, regards the differentiation of the impedance of the uRBC's curve from the impedance of the *Pf*-iRBC's curve for the lowest parasitemia, 0.031%. Such differentiation is greater in WB medium.

The convergence of the impedance of *Pf*-iRBC's curves towards the impedance of uRBC's curves, obtained for the various tests conducted, indicate the possibility of distinguishing the non-infected blood from blood infected with the malaria parasite for parasitemias between 0.0156-2 %, approximately 780-100 000 parasites per µl.

In comparison with the PCR technique, IS technique allows obtaining results more efficiently and in less time. However, the detection limit for PCR is approximately 0.05-10 parasites per µl corresponding to parasitemias between 0.000001-0.0002 %, distinct values of the values detected by IS technique. To detect submicroscopic infections, where exists very low parasite density (for example, 1-10 parasites per µl), is necessary proceed to new assays of IS for parasitemias similar to molecular technique ones [47, 48].

5. Conclusions

SEM, TEM and IS techniques demonstrate that nHz crystals coming from the sensitive strain 3D7 and from the resistant strain Dd2 of *P. falciparum* present a size, morphology and passive electrical properties that are more similar to the sHz crystals obtained using Protocol 2 than to those obtained using Protocol 1. This observation allows us to conclude that through the optimization of the experimental conditions of sHz crystals formation it is possible to obtain synthetic crystals that resemble the native ones. The optimization of crystal formation processes will contribute to the optimization of trials using antimalarial drugs that enable the formation of such crystals thus contributing to the production of drugs that diminish the parasite resistance to an antimalarial treatment.

The Impedance Spectroscopy (IS) devices proposed (low and high frequencies) demonstrate that it is possible to detect several or a single stage of *P. falciparum* in the peripheral blood. The detection allows to differentiate uninfected blood from Malaria-infected blood thus concluding that the IS technique could work as a diagnostic method. The impedance data obtained present high discrimination when the parallel and cross configurations are combined with a high frequency range. The low and high frequencies can be conjugated in order to find an ideal range for the measurement of the impedance data. Overall, the parallel configuration can be better to reproduce and obtain a dataset of impedance data more accurate than the cross configuration. However, in the last impedance results it is shown that both configurations can be applied for detection of malaria in human host.

6. References

1. Garcia LS: **Malaria**. *Clinics in laboratory medicine* 2010, **30**(1):93-129.

2. J Greenwood BM, Bojang K, Whitty CJ, Targett GA: **Malaria**. *Lancet* 2005, **365**(9469):1487-1498.

3. Miller LH, Baruch DI, Marsh K, Doumbo OK: **The pathogenic basis of malaria**. *Nature* 2002, **415**(6872):673-679.

4. Michalakis Y, Renaud F: **Malaria: Evolution in vector control**. *Nature* 2009, **462**(7271):298-300.

5. Egan TJ, Ncokazi KK: **Quinoline antimalarials decrease the rate of beta-hematin formation**. *Journal of inorganic biochemistry* 2005, **99**(7):1532-1539.

6. Solomonov I, Osipova M, Feldman Y, Baehtz C, Kjaer K, Robinson IK, Webster GT, McNaughton D, Wood BR, Weissbuch I *et al*: **Crystal nucleation, growth, and morphology of the synthetic malaria pigment beta-hematin and the effect thereon by quinoline additives: the malaria pigment as a target of various antimalarial drugs**. *Journal of the American Chemical Society* 2007, **129**(9):2615-2627.

7. Frosch T, Koncarevic S, Zedler L, Schmitt M, Schenzel K, Becker K, Popp J: **In situ localization and structural analysis of the malaria pigment hemozoin**. *The journal of physical chemistry B* 2007, **111**(37):11047-11056.

8. Rathore D, Jani D, Nagarkatti R, Kumar S: **Heme detoxification and antimalarial drugs – Known mechanisms and future prospects**. *Drug Discovery Today: Therapeutic Strategies* 2006, **3**(2):153-158.

9. Bohle DS, Kosar AD, Stephens PW: **Phase homogeneity and crystal morphology of the malaria pigment beta-hematin**. *Acta crystallographica Section D, Biological crystallography* 2002, **58**(Pt 10 Pt 1):1752-1756.

10. Hempelmann E: **Hemozoin biocrystallization in Plasmodium falciparum and the antimalarial activity of crystallization inhibitors**. *Parasitology research* 2007, **100**(4):671-676.

11. Kumar S, Guha M, Choubey V, Maity P, Bandyopadhyay U: **Antimalarial drugs inhibiting hemozoin (beta-hematin) formation: a mechanistic update**. *Life sciences* 2007, **80**(9):813-828.

12. Egan TJ, Chen JY, de Villiers KA, Mabotha TE, Naidoo KJ, Ncokazi KK, Langford SJ, McNaughton D, Pandiancherri S, Wood BR: **Haemozoin (beta-haematin) biomineralization occurs by self-assembly near the lipid/water interface**. *FEBS letters* 2006, **580**(21):5105-5110.

13. Fitch CD, Kanjananggulpan P: **The state of ferriprotoporphyrin IX in malaria pigment**. *The Journal of biological chemistry* 1987, **262**(32):15552-15555.

14. Slater AF, Swiggard WJ, Orton BR, Flitter WD, Goldberg DE, Cerami A, Henderson GB: **An iron-carboxylate bond links the heme units of malaria pigment**. *Proceedings of the National Academy of Sciences of the United States of America* 1991, **88**(2):325-329.

15. Bohle DS, Dinnebier RE, Madsen SK, Stephens PW: **Characterization of the products of the heme detoxification pathway in malarial late trophozoites by X-ray diffraction**. *The Journal of biological chemistry* 1997, **272**(2):713-716.

16. Egan TJ: **Biomimetic Approaches to Understanding the Mechanism of Haemozoin Formation**; 2011.

17. Oliveira MF, Kycia SW, Gomez A, Kosar AJ, Bohle DS, Hempelmann E, Menezes D, Vannier-Santos MA, Oliveira PL, Ferreira ST: **Structural and morphological characterization of hemozoin produced by Schistosoma mansoni and Rhodnius prolixus**. *FEBS letters* 2005, **579**(27):6010-6016.

18. Egan TJ: **Haemozoin formation**. *Molecular and biochemical parasitology* 2008, **157**(2):127-136.

19. Noland GS, Briones N, Sullivan DJ, Jr.: **The shape and size of hemozoin crystals distinguishes diverse Plasmodium species**. *Molecular and biochemical parasitology* 2003, **130**(2):91-99.

20. Hanscheid T, Egan TJ, Grobusch MP: **Haemozoin: from melatonin pigment to drug target, diagnostic tool, and immune modulator**. *Lancet Infect Dis* 2007, **7**(10):675-685.

21. Buller R, Peterson ML, Almarsson Ö, Leiserowitz L: **Quinoline binding site on malaria pigment crystal: a rational pathway for antimalaria drug design**. *Crystal growth & design* 2002, **2**(6):553-562.

22. Egan TJ: **Haemozoin (malaria pigment): a unique crystalline drug target**. *TARGETS* 2003, **2**(3):115-124.

23. Egan TJ: **Physico-chemical aspects of hemozoin (malaria pigment) structure and formation**. *Journal of inorganic biochemistry* 2002, **91**(1):19-26.

24. Pandey AV, Babbarwal VK, Okoyeh JN, Joshi RM, Puri SK, Singh RL, Chauhan VS: **Hemozoin formation in malaria: a two-step process involving histidine-rich proteins and lipids**. *Biochemical and biophysical research communications* 2003, **308**(4):736-743.

25. Tangpukdee N, Duangdee C, Wilairatana P, Krudsood S: **Malaria diagnosis: a brief review**. *The Korean journal of parasitology* 2009, **47**(2):93-102.

26. Cooke BM, Mohandas N, Coppel RL: **Malaria and the red blood cell membrane**. *Seminars in hematology* 2004, **41**(2):173-188.

27.http://www.cdc.gov/dpdx/resources/pdf/benchAids/malaria/Pfalciparum_benchaidV2.pdf

28. Greenwood BM, Fidock DA, Kyle DE, Kappe SH, Alonso PL, Collins FH, Duffy PE: **Malaria: progress, perils, and prospects for eradication**. *The Journal of clinical investigation* 2008, **118**(4):1266-1276.

29. Aditya NP, Vathsala PG, Vieira V, Murthy RS, Souto EB: **Advances in nanomedicines for malaria treatment**. *Advances in colloid and interface science* 2013, **201-202**:1-17.

30. Hafalla JC, Silvie O, Matuschewski K: **Cell biology and immunology of malaria**. *Immunological reviews* 2011, **240**(1):297-316.

31. Barsoukov E, Macdonald JR: **Impedance spectroscopy: theory, experiment, and applications**: John Wiley & Sons; 2005.

32. Slater AF, Swiggard WJ, Orton BR, Flitter WD, Goldberg DE, Cerami A, Henderson GB: **An iron-carboxylate bond links the heme units of malaria pigment**. *Proceedings of the National Academy of Sciences of the United States of America* 1991, **88**(2):325-329.

33. Trager W, Jensen JB: **Human malaria parasites in continuous culture**. *Science* 1976, **193**(4254):673-675.

34. Thaithong S, Seugorn A, Beale GH: **Culturing Plasmodium falciparum from finger-prick samples of infected blood**. *Transactions of the Royal Society of Tropical Medicine and Hygiene* 1994, **88**(4):490.

35. Cranmer SL, Magowan C, Liang J, Coppel RL, Cooke BM: **An alternative to serum for cultivation of Plasmodium falciparum in vitro**. *Transactions of the Royal Society of Tropical Medicine and Hygiene* 1997, **91**(3):363-365.

36. Fogel BJ, Shields CE, Von Doenhoff AE, Jr.: **The osmotic fragility of erythrocytes in experimental malaria**. *The American journal of tropical medicine and hygiene* 1966, **15**(3):269-275.

37. Shen SC, Fleming EM, Castle WB: **Osmotic and mechanical fragilities of erythrocytes of monkeys infected with P. knowlesi malaria**. *Proc Soc Exp Biol Med* 1946, **63**(2):419-422.

38. Lambros C, Vanderberg JP: **Synchronization of Plasmodium falciparum erythrocytic stages in culture**. *The Journal of parasitology* 1979, **65**(3):418-420.

39. Gildenhuys J, le Roex T, Egan TJ, de Villiers KA: **The single crystal X-ray structure of beta-hematin DMSO solvate grown in the presence of chloroquine, a beta-hematin growth-rate inhibitor**. *Journal of the American Chemical Society* 2013, **135**(3):1037-1047.

40. Fong KY, Wright DW: **Hemozoin and antimalarial drug discovery**. *Future medicinal chemistry* 2013, **5**(12):1437-1450.

41. Buller R, Peterson ML, Almarsson Ö, Leiserowitz L: **Quinoline binding site on malaria pigment crystal: a rational pathway for antimalaria drug design**. *Crystal growth & design* 2002, **2**(6):553-562.

42. Pagola S, Stephens PW, Bohle DS, Kosar AD, Madsen SK: **The structure of malaria pigment beta-haematin**. *Nature* 2000, **404**(6775):307-310.

43. Du E, Ha S, Diez-Silva M, Dao M, Suresh S, Chandrakasan AP: **Electric impedance microflow cytometry for characterization of cell disease states**. *Lab on a chip* 2013, **13**(19):3903-3909.

44. Ribaut C, Reybier K, Reynes O, Launay J, Valentin A, Fabre PL, Nepveu F: **Electrochemical impedance spectroscopy to study physiological changes affecting the red blood cell after invasion by malaria parasites**. *Biosensors & bioelectronics* 2009, **24**(8):2721-2725.

45. Ochola LB, Vounatsou P, Smith T, Mabaso ML, Newton CR: **The reliability of diagnostic techniques in the diagnosis and management of malaria in the absence of a gold standard**. *Lancet Infect Dis* 2006, **6**(9):582-588.

46. Okell LC, Ghani AC, Lyons E, Drakeley CJ: **Submicroscopic infection in *Plasmodium falciparum*-endemic populations: a systematic review and meta-analysis**. *The Journal of infectious diseases* 2009, **200**(10):1509-1517.

47. Garcia L: **Malaria Could You Recognize the World's Number Two Killer?**

48. Okell LC, Bousema T, Griffin JT, Ouedraogo AL, Ghani AC, Drakeley CJ: **Factors determining the occurrence of submicroscopic malaria infections and their relevance for control**. *Nature communications* 2012, **3**:1237.